EurjChem **Eur**opean **J**ournal of **Chem**istry

APH
ATLANTA PUBLISHING HOUSE

🔴 Check for updates

TD-DFT calculations, electronic structure, natural bond orbital analysis, nonlinear optical properties electronic absorption spectra and antimicrobial activity application of new *bis*-spiropipridinon/pyrazole derivatives

Shimaa Abdel Halim 🆔

Department of Chemistry, Faculty of Education, Ain Shams University, Roxy 11711, Cairo, Egypt
shimaaquantum@ymail.com (S.A.H.)

* *Corresponding author at: Department of Chemistry, Faculty of Education, Ain Shams University, Roxy 11711, Cairo, Egypt.*
Tel: +20.10.90306455 Fax: +20.11575.22581243 e-mail: shimaaquantum@ymail.com (S.A. Halim).

RESEARCH ARTICLE

ABSTRACT

A new *bis*-spiropipridinon/pyrazole compound and some of its derivatives are characterized in terms of several theoretical parameters such as density of states (DOS), molecular electrostatic potentials (MEPs), non-linear optical (NLO) properties and electrophilicity. The electronic structure and nonlinear optical properties of the studied compounds 1-5 are investigated theoretically at the DFT-B3LYP/6-311G(d,p) level of theory. The effect of substituents of different strengths on the geometry and energetic are analyzed and discussed. The static dipole moment (μ), polarizability (α), anisotropy polarizability ($\Delta\alpha$), and first order hyperpolarizability (β_{tot}), are parameters for NLO of the studied compounds have been calculated at the same level of theory and compared with the prototype *para*-nitro-aniline (PNA). The electronic absorption spectra of the studied compounds are recorded in the UV-VIS region, in both ethanol and dioxane solvents. The theoretical spectra computed at a new hybrid exchange-correlation functional using the Coulomb-attenuating method (CAM-B3LYP) at the 6-311G(d,p) bases set in gas phase and with the polarizable continuum model (PCM) in dioxane and ethanol indicate a good agreement with the observed spectra. The antimicrobial activity for studied compounds was investigated. The antimicrobial activity results revealed that compound 4 has a good potency against Gram positive bacteria (*E. coli*) and Gram negative bacteria (*P. vulgaris*) in comparison with doxymycin standard. The structure activity relationship SAR has been studied for the studied compounds by DFT calculations, moreover, confirmed practical antimicrobial activity results.

Cite this: *Eur. J. Chem.* **2018**, *9(4)*, 287-302 | **Journal website**: www.eurjchem.com

1. Introduction

Spiro heterocycles compounds having highly pronounced biological properties [1,2]. Spirooxindole ring systems were found in a number of alkaloids, such as horsifiline, spirotry-prostain, and (+) elacomine [3], and as inhibitors of the human NKI receptor [4], also; it used in biological applications as antimicrobial and antitumor agents. Furthermore, *bis*-hetero-cyclic compounds have been reported to possess interesting biological properties, [5-7] including antihypertensive, [8] antiallergenic, [9] and antitumor activities, [10,11]. Whereas, spirooxindole rings containing the pyrrolidine and pyrrolizine ring system were found in various natural products as fundamental nuclei and were well recognized for exhibiting a wide range of pharmacological and biochemical behaviors [12-14]. Therefore, the newly synthesized bioactive compounds *bis*-spiropipridinon/pyrazoleare useful compounds in creating distinct chemical libraries of drug-like molecules for biological screening [15,16]. The 1,3-cycloaddition methodology is one of the simplest tools for the construction of five-membered heterocycles [17]. Pyrazole derivatives have wide range of biological properties particularly being antifungal, antituber-cular, antibacterial, antiviral, anticancer and antioxidant, [18-22]. Pyrazole un-substituted in 1-position show NH acidity. The pK_a value of pyrazole is 14.21 and equal to that of imidazole [23].

There is no systematic study of the electronic structure, substituent effect and nonlinear properties. The NLO properties studied for understanding the biological activity of these molecules. Non-linear optical properties are the ability of any compound to convert light [with intense electric field (LASER)] of longer wavelength into light of shorter wavelength. One of the non-linear optical phenomena is the second harmonic generation (SHG) where intense light of longer wavelength is converted to half of the incident value, upon absorption by the non-linear optical material as shown in Figure 1.

Several investigations [11,17,24-28] have been published that dealt with the spectral characterization (IR, NMR, UV and X-ray) of *bis*-spiropipridinon/pyrazole derivatives.

The electronic structure and spectra of molecules usually manifests itself in the electronic absorption and emission spectra. This manifestation enables the detailed understanding of the forces that govern the electronic structure of the proposed structure of molecules, yet.
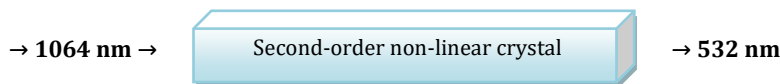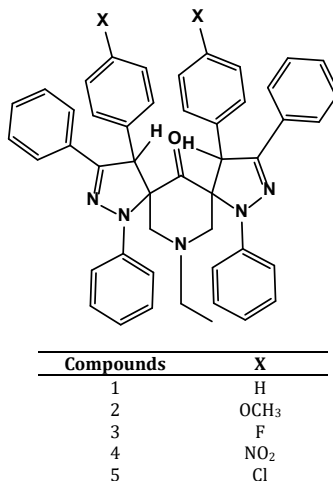
Figure 1. The second harmonic generation.

Compounds	X
1	H
2	OCH$_3$
3	F
4	NO$_2$
5	Cl

Figure 2. Schemes of the proposed structure of studied compounds **1**-**5**.

There is no systematic study of substituent and solvent effects on the observed spectra of *bis*-spiropipridinon/ pyrazole. Such a study is critically important in understanding their electronic structure, which may correlate with their biological activity.

The newly synthesized *bis*-spiropipridinon /pyrazole derivatives **1**-**5** are expected to have biological potential which needs to be explored by investigating their electronic structure and spectra experimentally and theoretically. The UV spectra and NBO analysis have been used to explain charge transfer within these molecules. The dependence of the electronic transitions of these molecules on the polarity of the solvent can be inferred from solvent-induced changes of such transitions, which is known as solvatochromism polarizable continuum model.

In the literature, there is no systematic study of the electronic structure, substituent effect and bonding characteristics of the studied compounds. Therefore, our contribution here is to shed more light on the geometrical parameters (bond lengths, bond angles and dihedral angles), ground state properties of the *bis*-spiropipridinon/pyrazole derivatives, energy gaps (highest occupied molecular orbital [HOMO]-lowest unoccupied molecular orbital [LUMO]), Natural charges, density of states, effect of substituents of different electron donating-withdrawing power in the two aryl moieties, and electrostatic potential are calculated using B3LYP/6-311G(d,p). The electronic dipole moment (μ), and first order hyperpolarizibility (β) values of the studied compounds have been computed to study the NLO properties to identify and characterize the forces that govern the structure-activity and the optical properties of the studied compounds. Finally, global reactivity descriptors including electronegativity (X), hardness (η), softness (S), and electrophilicity (ω) of the studied compounds were calculated and analyzed, while molecular electrostatic potential of molecules were explored as well.

The present work attempts to provide a detailed experimental (UV) using TD-DFT and theoretical electronic structure *bis*-spiropipridinon/pyrazole derivatives using CAM-B3LYP/6-311G(d,p). The biological activity of the studied compounds **2**-**5** was tested against Gram positive, Gram

negative and Fungi. The origin of each absorption band is identified and the contributing configurations and MOs are characterized. Natural bond orbital analysis is carried out to identify the extent of delocalization and the charge transfer of the electron density in the studied molecular systems and extent of conjugative interaction between different subsystems of the studied compounds. The effect of solvent polarity on the observed spectra and hence, predicting the relative stabilities, extent of charge transfers character and assignment of the observed electronic transitions are analyzed. The effect substituent's of different electron donating group (X = OCH$_3$) and electron withdrawing groups (X = F, NO$_2$ and Cl) on the electronic spectra of the studied compounds are discussed and analyzed.

2. Experimental

2.1. Synthesis

The compounds studied in this work are shown in Figure 2. The synthesis and characterization details of the compounds **1**-**5** are presents in literature [17].

2.2. Solvents

Polar (ethanol) and non-polar (dioxane) solvents were obtained from Merck, AR-grade, and were used without further purification.

2.3. Apparatus

The electronic absorption spectra were measured using a Perkin Elmer lambda 4B spectrophotometer using 1.0 cm fused quartz cells. The machine records linearly the percent of transmittance over the range 200-900 nm.

2.4. Antimicrobial study

Biological activities of synthesized *bis*-spiropipridinon/ pyrazole derivatives compounds were studied for antibacterial and antifungal properties against different types of bacteria;

Gram positive *S. aureus* (ATCC6538), and *E. coli* (ATCC10231) and Gram-negative *K. pneumonia (*ATCC 28737) and *P. vulgaris* (ATCC 547732), and *C. albicans* (ATCC 253674) for fungus.

2.5. Computational method

Calculations have been performed using Khon-Sham's DFT method subjected to the gradient-corrected hybrid density functional B3LYP method [29,30]. This function is a combination of the Becke's three parameters non-local exchange potential with the non-local correlation functional of Lee *et al.* [30]. For each structure, a full geometry optimization was performed using this function [30] and the 6-311G(p,d) basis set [31] as implemented by Gaussian 09 package [32]. All geometries were visualized either using GaussView 5.0.9 [33] or ChemCraft 1.6 [34] software packages.

The densities of states were calculated by using the GaussSum 2.2.5 program [35]. No symmetry constrains were applied during the geometry optimization. The electronic transition properties which include the maximum excitation wavelength (λ_{max}) and relative intensities (oscillator strengths, *f*), were obtained by the time dependant density functional theory (TD-DFT) [36] using "A new hybrid exchange-correlation functional using the Coulomb-attenuating method (CAM-B3LYP)," at the 6-311G(d,p) bases set [37]. The population analysis has also been performed by the natural bond orbital method [38] at B3LYP/6-311G(d,p) level of theory using natural bond orbital under Gaussian 09 program package. The second-order Fock matrix was used to evaluate the donor-acceptor interactions in the NBO basis [39]. For each donor (*i*) and acceptor (*j*), the stabilization energy E^2 associated with the delocalization $I \rightarrow j$ is estimated as

$$E^2 = \Delta E_{ij} = q_i \, (F \, (ij) \,^2 / \varepsilon_j - \varepsilon_i) \tag{1}$$

where q_i is the donor orbital occupancy, ε_i and ε_j are diagonal elements and (ij) is the off-diagonal NBO Fock matrix element. Also, the total static dipole moment (μ), $\langle \Delta \alpha \rangle$, $\langle \beta \rangle$, values were calculated by using the following equations [40-42];

$$\mu = (\mu^2_x + \mu^2_y + \mu^2_z)^{\frac{1}{2}} \tag{2}$$

$$\langle \alpha \rangle = 1/3(\alpha_{xx} + \alpha_{yy} + \alpha_{zz}) \tag{3}$$

$$\Delta \alpha = ((\alpha_{xx} - \alpha_{yy})^2 + (\alpha_{yy} - \alpha_{zz})^2 + (\alpha_{zz} - \alpha_{xx})^2/2)^{1/2} \tag{4}$$

$$\langle \beta \rangle = (\beta^2_x + \beta^2_y + \beta^2_z)^{1/2} \tag{5}$$

where, $\beta_x = \beta_{xxx} + \beta_{xyy} + \beta_{xzz}$, $\beta_y = \beta_{yyy} + \beta_{xxy} + \beta_{yzz}$, $\beta_z = \beta_{zzz} + \beta_{xxz} + \beta_{yyz}$.

By using HOMO and LUMO energy values, electronegativity, and chemical hardness can be calculated as follows: $\chi = (I + A)/2$ (electronegativity), $\eta = (I - A)/2$ (chemical hardness), $S = 1/2\eta$ (global softness), $\omega = \mu^2/2\eta$ (electrophilicity) where I and A are ionization potential and electron affinity, and $I = -E_{HOMO}$ and $A = -E_{LUMO}$, respectively [43,44]. The conversion factors for α, β and HOMO and LUMO energies in atomic and cgs units: 1 atomic unit (a.u.) = 0.1482×10^{-24} electrostatic unit (esu) for polarizability; 1 a.u. = 8.6393×10^{-33} esu for first hyperpolarizability $\langle \beta \rangle$; 1 a.u. = 27.2116 eV (electron volt) for HOMO and LUMO energies.

3. Results and discussion

3.1. Geometric parameters

The optimized structure of the parent molecule **1** and the effect of substituent of different electron donating/withdrawing power at C53-Ph-X and C92-Ph-X on the geometrical

parameters (bond lengths, bond angles and dihedral angles) of the studied compounds **2**-**5**, is listed in Tables 1 and 2.

The computed bond lengths and bond angles are compared with the available experimental data [45-47]. Figure 3 presented the global energy minimum obtained by the DFT-B3LYP/6-311G(d,p) and the vector of the dipole moment. The calculated bond lengths C1-N4 and N4-C3 of the *bis*-spiro-pipridinon/pyrazole are underestimated than the experimental values by 1%, whereas, the computed C3-C16 and C2-C16 bond lengths are overestimated than the experimental values by 1%. At the same time, the computed C17-N18, C58-N56 and C54-N57 bond lengths are overestimated than the experimental values by 1%, while C16-N19 and C92-C42 is underestimated than the experimental values by 1%. The small difference between calculated and observed bond lengths indicates the power of the method used in calculation. No significant change in the calculated bond angles of the studied compounds **1**-**5** on comparing with the experimental values. The small difference between calculated and observed angles may be attributed to that the calculations were carried out in gas phase and observed in solid state. All the studied compounds **1**-**5** are non-planner as reflected from their dihedral angles. In the parent compound **1**, the C53-Ph and C92-Ph moieties are out of the molecular plane of the *bis*-spiropipridinon/pyrazole by dihedral angles equal 91.67° for C1-C58-C53-C81 and 19.79° for C3-C16-C92-C42, respectively. Upon substitution no significant change in the dihedral angles of the C53-Ph-X while the dihedral angles of C92-Ph-X moiety decreased and become nearly planner (c.f. Tables 1 and 2).

3.2. Natural charge analysis

Natural charge analysis is performed on the electronic structures clearly describes the distribution of electrons in various sub shells of their atomic orbital's [48]. Table 2 show that; the natural charges and natural populations for the studied compounds **1**-**5** calculated at B3LYP/6-311G(d,p) level of theory. For the parent compound **1**, the most electronegative charges are accumulated on N4, O7, C9, N18, N19, N56 and N57. According to an electrostatic point of view of the molecule, these electronegative atoms have a tendency to donate electrons. Whereas, the most electropositive atoms such as; C2 and C17 have a tendency to accept electrons in Table 2. The corresponding Mullikan's plot with B3LYP/6-311G(d,p) method are shown in Figure 4. It is noted that from Figure 4, the strong negative and positive partial charges on the skeletal atoms of the parent (especially C2, N4, O7, C9, C17, N18, N19, N56 and N57) increases with increasing Hammett constant of substituent groups. These distributions of partial charges on the skeletal atoms show that the electrostatic repulsion or attraction between atoms can give a significant contribution to the intra- and intermolecular interaction.

3.3. Global reactivity descriptors

They include HOMO, LUMO, energy gap (E_g), chemical hardness (η), electronegativity (X), chemical potential (V), electrophilicity (ω), electron affinity (A), ionization potential (I) and global softness (S) which are calculated at B3LYP/6-311G(d,p). The studied compounds were calculated the frontier molecular orbital (FMO) energies at the same level of theory. The electron donating ability characterized by HOMO energy, while LUMO energy characterizes the electron withdrawing ability. Energy gap (E_g) between HOMO and LUMO characterizes the molecular chemical stability, which is a critical parameter in determining molecular electrical transport properties because it is a measure of electron conductivity. The results in Figures 5, 6 and Table 3 indicate that the smaller the energy gap the easier the charge transfer and the polarization occurs within the molecule.

Table 1. Selected experimental and theoretical bond lengths and bond angles for the studied compounds **1**-**5** computed at the B3LYP/6-311G(d,p) level of theory.

Parameters	Experimental [45-47]	Compound				
		1	2	3	4	5
Bond lengths (Å)						
C_1-N_4	1.361	1.350	1.378	1.351	1.342	1.351
N_4-C_3	1.343	1.332	1.303	1.331	1.333	1.331
C_3-C_{16}	1.471	1.486	1.475	1.486	1.479	1.485
C_{16}-C_2	1.565	1.566	1.572	1.567	1.575	1.566
C_2-C_{58}	1.565	1.570	1.568	1.569	1.564	1.570
C_2-O_7	1.212	1.202	1.192	1.201	1.199	1.202
N_4-C_8	1.505	1.491	1.490	1.491	1.502	1.491
C_8-C_9	1.471	1.525	1.526	1.525	1.524	1.525
C_{16}-N_{19}	1.505	1.476	1.472	1.474	1.466	1.475
N_{18}-N_{19}	1.385	1.359	1.349	1.361	1.367	1.359
N_{18}-C_{17}	1.275	1.287	1.281	1.287	1.289	1.287
C_{92}-C_{42}	1.565	1.520	1.519	1.520	1.523	1.519
C_{17}-C_{31}	1.471	1.467	1.467	1.466	1.456	1.466
N_{19}-C_{20}	1.395	1.404	1.389	1.406	1.412	1.405
C_{58}-N_{56}	1.505	1.524	1.525	1.524	1.485	1.525
N_{56}-N_{57}	1.385	1.361	1.361	1.361	1.360	1.362
N_{57}-C_{54}	1.275	1.286	1.292	1.286	1.297	1.286
C_{53}-C_{54}	1.515	1.526	1.525	1.526	1.534	1.527
C_{53}-C_{81}	1.515	1.513	1.509	1.512	1.512	1.512
C_{54}-C_{70}	1.471	1.469	1.472	1.468	1.463	1.468
N_{56}-C_{59}	1.395	1.417	1.416	1.417	1.427	1.417
Bond angles (°)						
<C_1-N_4-C_3	125.00	126.50	126.70	126.35	126.16	126.44
< N_4-C_3-C_{16}	120.99	119.28	119.95	119.07	121.00	119.25
<C_3-C_{16}-C_2	109.31	111.29	112.05	111.28	111.43	111.66
<C_{16}-C_2-C_{58}	120.00	118.34	118.56	118.13	119.22	118.32
<C_{58}-C_2-O_7	119.99	120.89	120.61	121.02	120.67	120.99
<C_3-N_4-C_8	115.95	116.76	118.11	116.85	116.84	116.88
<N_4-C_8-C_9	115.80	113.03	113.01	113.06	112.54	113.01
<C_2-C_{16}-N_{19}	110.96	110.55	110.53	110.74	109.85	110.78
<C_{20}-$N_{18}$$N_{19}$	119.55	118.63	118.64	118.51	118.18	118.64
< $N_{18}$$N_{19}$-$C_{17}$	110.69	110.10	111.60	110.96	110.87	111.07
< N_{18}-$C_{17}$$C_{92}$	109.41	112.69	112.27	112.59	112.28	112.60
<C_{17}-C_{92}-C_{16}	97.411	99.77	99.60	99.69	99.47	99.79
<C_{92}-C_{16}-C_2	107.99	106.50	106.20	106.32	108.14	105.91
<C_{16}-N_{19}-C_{20}	127.61	128.79	128.60	128.75	128.82	128.72
<N_{18}-C_{17}-C_{31}	125.00	121.26	121.70	121.56	121.96	121.49
<C_{92}-C_{17}-C_{31}	125.99	125.99	125.97	125.80	125.74	125.84
<C_{16}-C_{92}-C_{42}	115.92	114.69	115.17	114.83	113.52	114.71
<C_2-C_{58}-N_{56}	105.00	106.24	106.23	106.21	107.33	106.18
<C_{58}-N_{56}-N_{57}	112.95	111.87	111.74	111.78	113.08	111.67
<C_{54}-C_{53}-C_{58}	100.36	102.22	101.95	102.17	101.02	102.18
<C_{53}-C_{58}-C_1	117.96	112.22	111.83	112.24	113.29	112.23
<N_{57}-N_{56}-C_{59}	117.99	116.68	116.85	116.70	116.54	116.69
<C_{58}-N_{56}-C_{59}	125.99	125.75	125.69	125.82	127.34	125.96
<N_{57}-C_{54}-C_{70}	120.00	120.70	120.59	120.77	120.86	120.80
<C_{53}-C_{54}-C_{70}	125.99	126.89	126.97	126.88	127.28	127.03
<C_{54}-C_{53}-C_{81}	117.80	116.85	117.68	117.10	117.56	117.31

Furthermore, the order of increasing reactivity in the studied compounds is **4** > **5** > **1** > **3** > **2**. The insignificant differences in E_g of all the studied compounds except **4** is due to the non-planarity of the two Ph-X and Ph-X with the *bis*-spiropipridinon/pyrazole (c.f. Table 3). Using HOMO and LUMO energies, ionization potential and electron affinity can be expressed as I~ -E_{HOMO}, A~ -E_{LUMO} at the B3LYP/6-311G (d,p) as shown in Table 3. The variation of electronegativity (*X*) values is supported by electrostatic potential, for any two molecules, where electron will be partially transferred from one of low *X* to that of high *X*. The results show that the order of decreasing *X* is **2** < **1** < **3** < **5** < **4**. The chemical hardness (η) = (I-A)/2, electronegativity (*X*) = (I+A)/2, chemical potential (V) = -(I+A)/2, electrophilicity (ω) = μ^2/ 2η and global softness (S) = 1/2η values are calculated and presented in Table 3. The results of small η values for the studied compounds reflect the ability of charge transfer inside the molecule. Therefore, the order is **4** > **5** > **1** > **3** > **2**. There is a linear relationship between η and E_g as shown in Table 3. Considering η values, the higher the η values, the harder is the molecule and vice versa.

3.4. Nonlinear optical analysis

So far, no experimental or theoretical investigations were found addressing NLO for these classes of molecules; therefore, this triggered our interest to undertake this study. The relationship between molecular structure and NLO, the polarizibilities and hyperpolarizibilities of the studied compounds **1-5** are calculated using DFT/B3LYP/6-311G(d,p) investigated by NLO due to its importance in providing key functions of frequency shifting, optical modulation, switching , laser, fiber, optical materials logic and optical memory for the emerging technologies in areas such as telecommunications, signal processing and optical inter connections [49]. In order to investigate the relationship between molecular structure and NLO, the polarizibilities and hyperpolarizibilities of the studied compounds **1-5** are calculated using DFT/B3LYP/6-311G(d,p). Total static dipole moment (μ), the mean polarizability (α), the anisotropy of the polarizability $\Delta\alpha$, the mean first-order hyperpolarizibility (β) of the studied compounds **1-5** are listed in Table 4.

Table 2. Dihedral angles and natural charge for the studied compounds **1-5** computed at the B3LYP/6-311G(d,p) level of theory.

Parameters	Compounds				
	1	**2**	**3**	**4**	**5**
Dihedral angles (°)					
$<C_1N_4C_3C_{16}$	10.04	9.697	10.07	6.335	9.863
$<N_4C_3C_{16}C_2$	-33.20	-31.59	-34.13	-23.08	-32.61
$<C_3C_{16}C_2C_{58}$	31.45	29.72	31.98	26.33	30.20
$<C_{16}C_2C_{58}C_1$	-8.17	-7.479	-7.552	-13.77	-6.739
$<C_{58}C_1N_4C_3$	18.09	16.98	19.38	9.389	18.43
$<C_1N_4C_8C_9$	-76.15	-74.08	-74.43	-78.34	-74.15
$<C_3N_4C_8C_9$	101.92	103.97	103.69	100.19	104.15
$<O_7C_2C_{16}C_3$	-147.36	-149.40	-147.16	-155.06	-149.20
$<O_7C_2C_{58}C_1$	170.64	171.65	171.59	167.63	172.65
$<O_7C_2C_{16}N_{19}$	-20.27	-21.92	-19.64	-28.64	-21.64
$<N_{19}N_{18}C_{17}C_{92}$	4.193	4.563	4.049	6.311	4.202
$<N_{18}C_{17}C_{92}C_{16}$	-14.92	-15.97	-15.50	-17.55	-14.91
$<C_{17}C_{92}C_{16}C_2$	-96.76	-96.34	-95.88	-94.38	-96.82
$<C_{17}N_{18}N_{19}C_{20}$	-173.70	-174.56	-176.28	-179.54	-174.38
$<C_{20}N_{19}C_{16}C_{92}$	166.00	166.72	168.75	170.88	166.76
$<N_{18}C_{17}C_{92}C_{42}$	106.99	107.11	106.44	103.00	107.01
$<C_{42}C_{92}C_{16}C_2$	143.07	143.37	144.16	145.69	143.06
$<C_1C_{58}N_{56}N_{57}$	139.83	141.30	140.21	139.36	141.30
$<N_{56}N_{57}C_{54}C_{53}$	-0.252	-0.725	-0.428	-3.385	-0.768
$<N_{57}C_{54}C_{53}C_{58}$	13.70	15.23	14.04	15.48	15.16
$<C_{59}N_{56}N_{57}C_{54}$	-169.65	-170.50	-169.72	-173.81	-170.43
$<C_2C_{58}N_{56}C_{59}$	55.494	56.899	55.93	61.62	57.22
$<N_{57}C_{54}C_{53}C_{81}$	144.31	146.67	144.48	146.07	146.12
Natural charge					
C2	0.61085	0.61228	0.61180	0.61503	0.61139
N4	-0.27847	-0.27538	-0.27941	-0.27638	-0.27833
O7	-0.52662	-0.52547	-0.52754	-0.52572	-0.52798
C9	-0.57826	-0.57823	-0.57780	-0.57776	-0.57771
C17	0.21806	0.21732	0.21765	0.21925	0.21683
N18	-0.24114	-0.24412	-0.24205	-0.24349	-0.24124
N19	-0.25674	-0.24908	-0.25735	-0.26110	-0.25643
N56	-0.28791	-0.29010	-0.28930	-0.29207	-0.29066
N57	-0.23088	-0.23608	-0.23191	-0.22736	-0.23192
O93	-	-0.52688	-	-0.14489	-
O94	-	-0.52254	-	-0.14787	-
F91	-	-	-0.34924	-	-
F92	-	-	-0.34882	-	-
N91	-	-	-	0.08605	-
N92	-	-	-	0.09283	-
O95	-	-	-	-0.15628	-
O96	-	-	-	-0.14353	-
Cl91	-	-	-	-	-0.00988
Cl92	-	-	-	-	-0.00732

The polarizibilities, and first-order hyperpolarizibilities are reported in atomic units (a.u.), the calculated values have been converted into electrostatic units (esu) using conversion factor of 0.1482×10^{-24} esu for α and 8.6393×10^{-30} esu for β. The standard prototype of *p*-nitro aniline is used in NLO studies, which chosen as a reference as there were no experimental values of NLO properties of the studied compounds. The values of α, β in Table 4 show that the order of increasing α with respect to PNA is: compounds **4** and **5** are ~3 times higher than PNA, compounds **2** and **3** are ~2.5 times higher than the standard, whereas compound **1** is ~1.5 times higher than PNA, respectively, The calculated first order hyperpolarizability of *p*-nitro-acetanilide is 15.482×10^{-30} esu as reported by T. Gnanasambandan *et al.* [50-52]. The analysis of the β parameter show that compounds **1** and **3** are ~2.0 and 2.5 times higher than *p*-nitro-acetanilide, while compounds **2**, **4** and **5** are ~1.8, 1.3 and 0.7 times higher than the reference, respectively.

3.5. Density of states

The density of states of a system describes the number of states per interval of energy at each energy level that are available to be occupied by electrons. A high DOS at a specific energy level means that there are many states available for occupation. The calculated DOS are presented in Figure 7 to clarify the effects of the studied compounds **1-5**. As shown, DOS becomes more abundant near Fermi levels in both NO_2

(**4**) and Cl (**5**), where the overall features of DOS change, and deep vales develop on both sides nearby Fermi levels.

3.6. Molecular electrostatic potential

The electronic density is related to the molecular electrostatic potential and this is a very useful descriptor in understanding sites for electrophilic and nucleophilic attack as well as hydrogen bonding interactions [53]. MEP is correlated with dipole moments, electro negativity, partial charges and chemical reactivity of the molecules. These maps allow us to visualize variably charged regions of a molecule. Knowledge of the charge distributions can be used to determine how molecules interact with one another. The calculated 3D MEP of the studied compounds **1-5** are calculated from optimized molecular structure using DFT/B3LYP/6-311G(d,p) are shown in Figure 8. The results show that , in case of compound **1** (X = H) the negative region (red) is mainly over the N and O atomic sites, which is caused by the contribution of lone-pair electrons of nitrogen and oxygen atoms while the positive (blue) potential sites are around the hydrogen and carbon atoms. A portion of the molecule that has negative electrostatic potential will be susceptible to electrophilic attack-the more negative the higher the tendency for electrophilic attack. The color scheme for the MEP surface is as follows: red for electron rich, (partially negative charge); blue for electron deficient, (partially positive charge); light blue for (slightly electron deficient region); yellow for (slightly electron rich region);
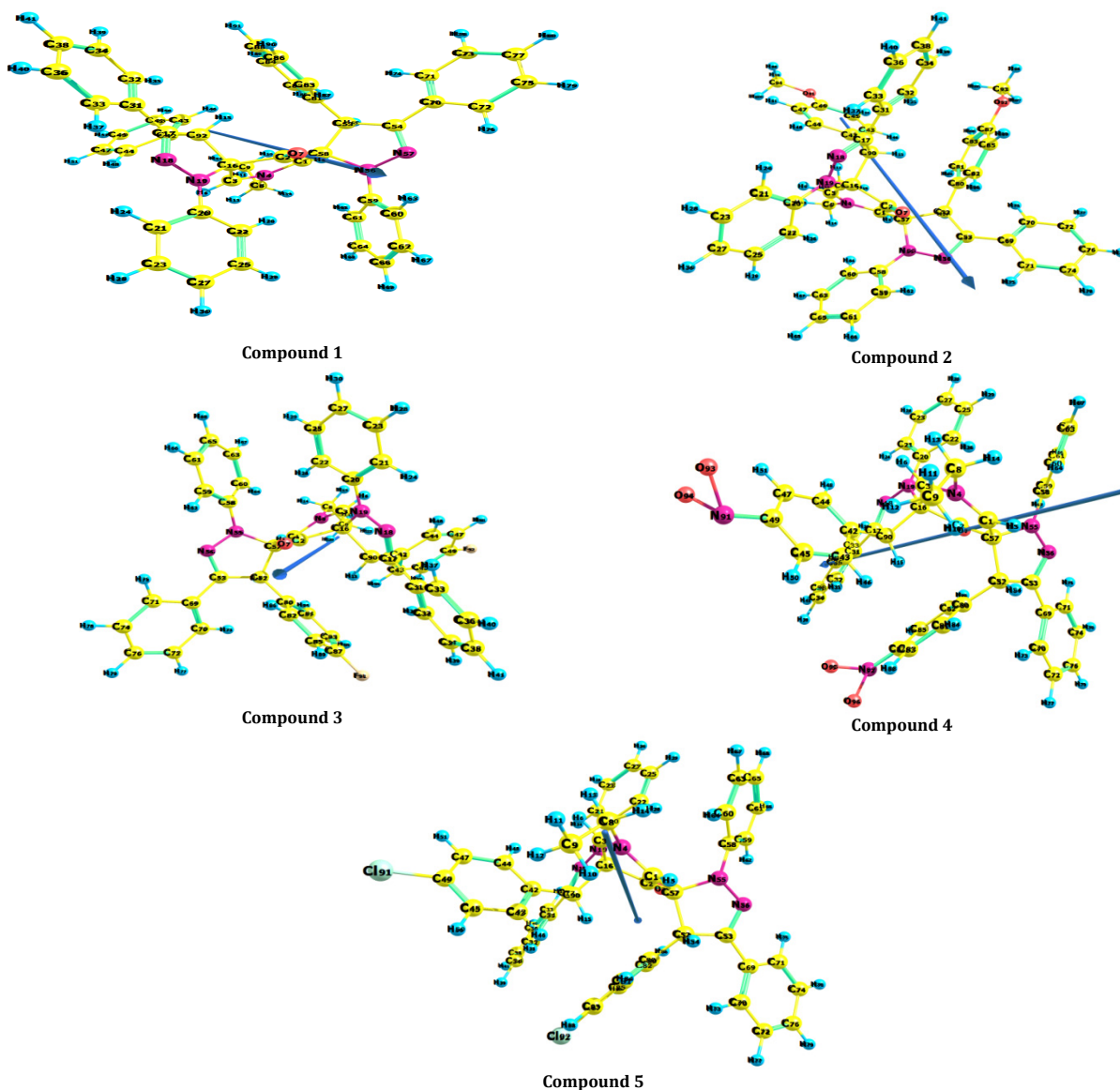
Figure 3. Optimized geometry, vector of the dipole moment and numbering system, for the studied compounds **1**-**5** at B3LYP/6-311G(d,p).
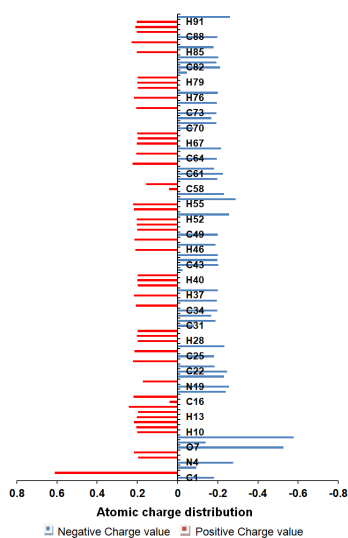

Figure 4. Atomic charge distribution (au) for compound **1** at B3LYP/6-311G(d,p) basis set.

green for neutral (zero potential), respectively. Potential increases in the following order: red < orange < yellow < green < blue [54,55].

3.7. Electronic absorption spectra of compound 1

The theoretical electronic absorption spectra of compound **1** in dioxane and ethanol are presented in Figure 9 and Table S1. The spectrum of compound **1** is composed of six bands in the range 200-500 nm. The bands are assigned as π-π* transitions, as indicated by the values of molar absorptive (ε = 0.000-70.000). In order to account for the theoretically UV Spectra of compound **1** in dioxane and ethanol, using TD-DFT-CAM-B3LYP/6-311G(d,p) level. The theoretical band by using PCM (dioxane), at 337.7 nm (State I), and in gas phase at 336.2 nm as shown in Table S1. The theoretical calculations of single point energy vertical excitations in ethanol reproduce the wavelength of this band at 336.2 nm (State I). The second band is reproduced theoretically at 320.4 nm in dioxane (State II). The gas phase calculation gives a wavelength at 323.6 nm. Moreover, theoretical gas phase wavelength is even higher than the theoretical wavelength in dioxane.

Table 3. Total energy, energy of HOMO and LUMO, energy gap, dipole moment, the ionization potential (I), electron affinity (A), chemical hardness (η), global softness (S), chemical potential (V), electronegativity (χ), and global electrophilicity index, (ω) of the studied compounds **1-5** computed at the B3LYP/6-311G(d,p) .

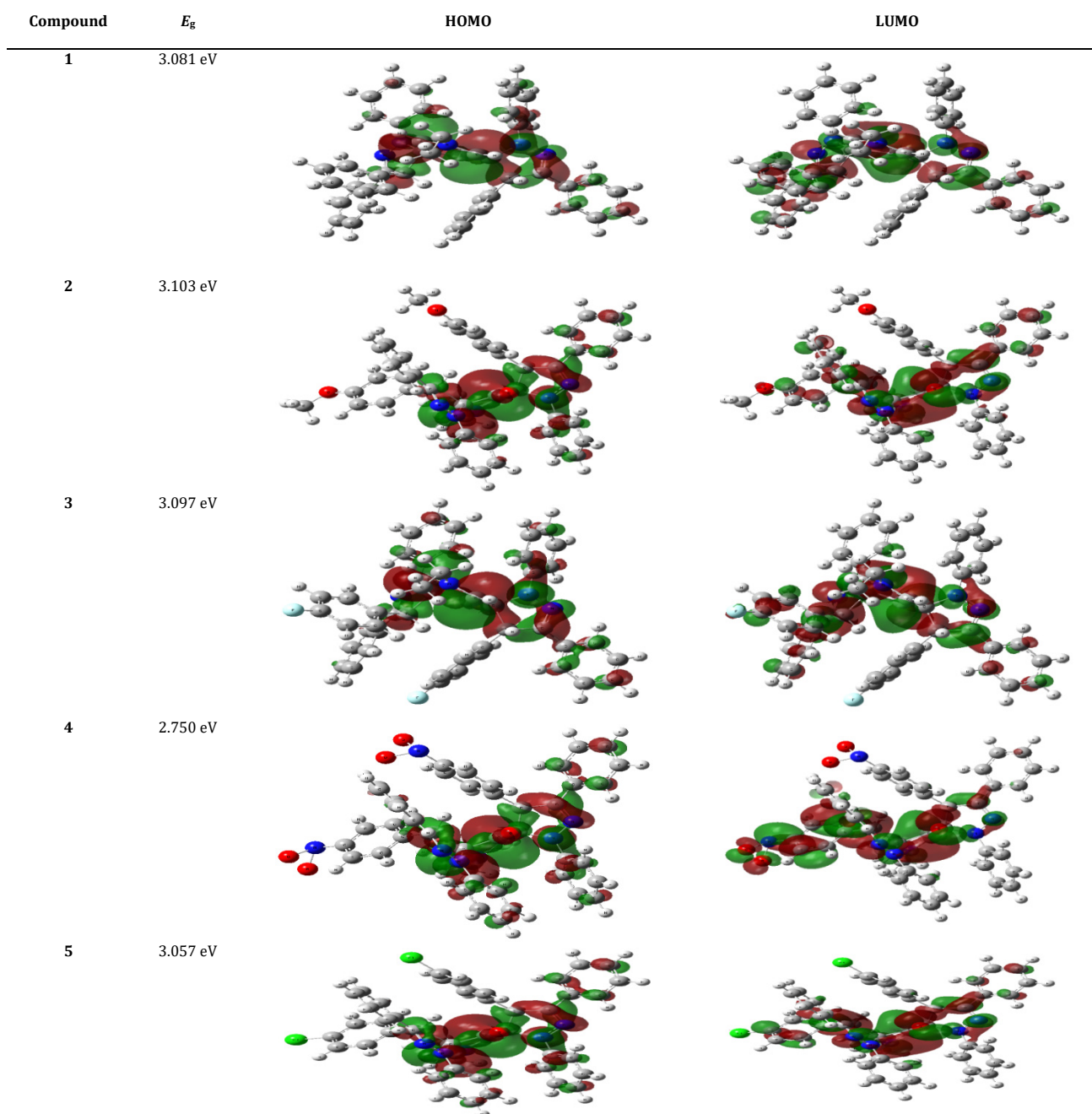| Compounds	1	2	3	4	5
E_T (au)	-2163.8473	-2392.9516	-2362.3761	-2572.6944	-3083.0904
E_{HOMO} (eV)	-4.77278	-4.67487	-4.90742	-4.83834	-4.95448
E_{LUMO} (eV)	-1.69211	-1.57189	-1.81070	-2.08842	-1.89693
E_{gap} (eV)	3.08067	3.10298	3.09672	2.74992	3.05755
μ (Debye)	6.2817	8.1570	4.8285	4.6366	4.5527
I (eV)	4.77278	4.67487	4.90742	4.83834	4.95448
A (eV)	1.69211	1.57189	1.81070	2.08842	1.89693
X (eV)	3.23244	3.12338	3.35906	3.46338	3.42571
V (e/V)	-3.23244	-3.12338	-3.35906	-3.46338	-3.42571
η (eV)	1.54033	1.55149	1.54836	1.37496	1.52878
S (e/V)	0.32461	0.32227	0.32292	0.36365	0.32706
ω (eV)	3.39170	3.14391	3.64362	4.36194	3.83819

Compound	E_g	HOMO	LUMO
1	3.081 eV		
2	3.103 eV		
3	3.097 eV		
4	2.750 eV		
5	3.057 eV		

Figure 5. HOMO, LUMO and Energy gap of the studied compounds **1-5** at B3LYP/6-311G(d,p).

Table 4. Total static dipol moment (μ), the mean polarizability ($<\alpha>$), the anisotropy of the polarizability ($\Delta\alpha$), and the mean first-order hyperpolarizability ($<\beta>$), for the studied compounds **1-5** computed at B3LYP/6-311G(d,p).

Properties	PNA	Compounds				
		1	2	3	4	5
μ_x, D		-2.1739	-5.6599	-0.7443	2.2384	-0.4205
μ_y, D		-1.2024	0.4318	0.4573	-1.2747	-1.0215
μ_z, D		5.7696	-5.8580	4.7488	-3.8552	-4.4167
μ, Debye [a]	2.44	6.2817	8.1570	4.8284	4.6366	4.5527
α_{XX}, a.u.		-314.867	-322.8623	-333.341	-376.969	-351.749
α_{XY}, a.u.		-1.1187	-0.9886	-2.2939	-3.0178	-0.4535
α_{YY}, a.u.		-287.833	-304.6026	-303.890	-333.865	-321.722
α_{ZZ}, a.u.		-286.0357	-318.8137	-299.618	-320.691	-316.710
α_{YZ}, a.u.		4.2840	5.1291	4.9584	5.2993	5.1896
α_{XZ}, a.u.		-8.0905	10.8510	0.1248	-6.3859	-1.5989
$<\alpha>\times10^{-24}$ esu [a]	22.0	43.90	46.75	46.28	49.96	48.91
$\Delta\alpha\times10^{-24}$ esu		47.74	40.52	49.17	45.98	49.97
β_{XXX}, a.u.		-44.0373	-240.173	-3.1945	130.646	49.1193
β_{XXY}, a.u.		-28.3853	170.091	-29.1253	29.0326	21.8505
β_{XYY}, a.u.		-46.8852	-126.586	22.3072	101.547	47.3975
β_{YYY}, a.u.		95.6148	42.3811	32.3884	-67.9147	-65.1408
β_{XXZ}, a.u.		15.8096	61.9425	-103.091	139.9476	111.564
β_{XYZ}, a.u.		-14.9060	-15.2491	-7.8688	28.1463	6.9155
β_{YYZ}, a.u.		-65.0225	-45.3843	34.2251	-28.6670	-27.3395
β_{XZZ}, a.u.		-46.4699	33.8242	-19.2609	-18.1681	-23.7194
β_{YZZ}, a.u.		-20.1235	-32.3737	-2.9841	-5.2738	-4.9764
β_{ZZZ}, a.u.		65.7684	-40.0246	52.2643	-31.2953	-33.3131
$<\beta>\times10^{-30}$ esu [a]	15.5	38.38	22.60	23.19	21.10	17.49

[a] PNA results are taken from references [50-52].

In ethanol, this same band appears at 322.8 nm, (State II), as shown in Table S1. The third $(\pi\text{-}\pi^*)^1$ state theoretically at 315.8 nm in dioxane, (State III), which involves the orbital's φ_{181} and φ_{184}, in the transition. The gas phase calculation gives a wavelength at 318.2 nm (State III), which also involves orbital's φ_{182} and φ_{184}. In ethanol, this same band appears at 317.0 nm, (State III), as shown in Table S1. The fourth $(\pi\text{-}\pi^*)^1$ state theoretically at 303.1 nm (State IV) in dioxane. The gas phase calculations gives a wavelength at 305.4 nm (State IV), which also involves orbital's φ_{181} and φ_{184}.
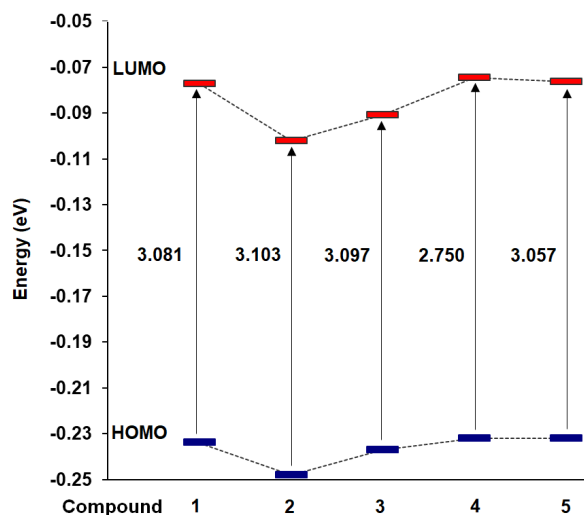

Figure 6. Energy of HOMO, LUMO and energy gap of the studied compounds **1-5** at B3LYP/6-311G(d,p) level of theory.

In ethanol, this same band appears at 305.3 nm, as shown in Table S1, which involves the orbital's φ_{181} and φ_{184} in the transition. The five $(\pi\text{-}\pi^*)^1$ state theoretically at 290.7 nm (State V) in both dioxane, gas phase and ethanol, which also involves orbital's φ_{182} and φ_{186}, as shown in Table S1. The six $(\pi\text{-}\pi^*)^1$ state theoretically at 281.1 nm (State VI) in dioxane. The gas phase calculations give a wavelength at 283.1 nm (state VI), which also involves orbital's φ_{180} and φ_{185}. In ethanol, this same band appears at 282.9 nm, as shown in Table S1. The nature of the electronic transition can be

inferred from examining the electron density contours of molecular orbitals. The seven orbital's φ_{180}, φ_{181}, φ_{182}, φ_{183}, φ_{184}, φ_{185}, and φ_{186}, respectively, involved in the theoretical transitions of compound **1**, are shown in Figure S1, where the first , second and third bands involving φ_{180} and φ_{183} & φ_{182} and φ_{185} & φ_{182} and φ_{184} show a delocalization of electron density and a Charge Transfer CT character, while the fourth, five and six bands involving φ_{181} and φ_{184} & φ_{182} and φ_{186} & φ_{180} and φ_{185} shows a Charge Transfer CT character.

The NBO analysis of the studied compounds **1-5** provides an efficient method for studying intra-and intermolecular bonding and also provides a convenient basis for investigating charge transfer or conjugative interactions in molecular systems. Table 5 presents the second order perturbation energies (often called as the stabilization energies or interaction energies) of most interacting NBOs of compounds **1-5** and the most important interaction between filled (donor) Lewis type NBOs and empty (acceptor) non-Lewis NBOs. The charge density maps of HOMO and LUMO for compounds **1-5** are presented in Figure 7. The results of NBO analysis of compound **1** tabulated in Table 5 indicate that there is a strong hyper conjugative interactions LP(1) $C_3 \rightarrow \pi^*C_1\text{-}N_4$, $\pi^*C_{17}\text{-}N_{18} \rightarrow \pi^*C_{31}\text{-}C_{32}$, LP(1) $N_{19} \rightarrow \pi^*C_{20}\text{-}C_{22}$, LP(1) $N_{56} \rightarrow \pi^*C_{54}\text{-}N_{57}$, and LP(2) $O_7 \rightarrow \sigma^*C_2\text{-}C_{16}$, for compound **1** is 255.11, 142.50, 33.66, 27.01 and 23.13 kcal/mol, respectively. The C–N π orbital in two pyrazole and *bis*-spiropipridinon groups interacts equally well with *bis*-spiropipridinon/pyrazole ring. In fact, its interaction with the pyrazole ring is greater. Furthermore, the lone pair orbital of the nitrogen atom enjoys hyperconjugation with the C2–O7, C1–C57 and C3–C16 π^* orbital. It is surprising to notice a decrease in the population of the NBO C31–C32, C17–N18, and C59–C61 reflecting a charge transfer away from *bis*-spiropipridinon/pyrazole ring. This is also evident in the case of the population of the carbon lone orbital LP(1) C3. In conclusion, compound **1** enjoys the linear conjugation that is responsible for the observed spectrum. No specific part of the molecule manifests itself in the observed spectrum.

3.8. Electronic absorption spectra of compound 2

Insertion of two OCH$_3$ groups in position two X in two Ph-X of compound **1** gives compound **2**. The experimental and theoretical electronic absorption spectra of compound **2** in dioxane and ethanol are shown in Figure 10 and Table S2.

Table 5. Second order perturbation interaction energy values computed in the NBO basis for the studied compounds **1-5** calculated at B3LYP/6-311G(d,p).

Compound	Donor	Acceptor	E^2 (kcal/mol) [a]	NBO	Population
1	πC1-N4	LP(1) C3	18.38	C1-N4	1.93901
	πC20-C22	π*C25-C27	22.50	C20-C22	1.64741
	πC31-C32	π*C17-N18	18.77	C31-C32	1.63606
	LP(1) C3	π*C1-N4	255.11	LP(1) C3	1.19275
	LP(1) O7	RY*C2	15.79	LP(1) O7	1.97434
	LP(2) O7	σ*C2-C16	23.13	LP(2) O7	1.86809
	LP(1) N19	π*C17-N18	30.92	LP(1) N19	1.67886
	LP(1) N19	π*C20-C22	33.66	LP(1) N56	1.72398
	LP(1) N56	π*C54-N57	27.01	C17-N18	0.23646
	LP(1) N56	π*C59-C61	13.78	C59-C61	0.38910
	π*C17-N18	π*C31-C32	142.50	-	-
	π*C59-C61	π*C60-C62	254.14	-	-
2	πC1-N4	LP(1) C3	22.20	C1-N4	1.93361
	πC1-N4	π*C1-N4	12.22	LP(1) C3	1.14759
	LP(1) C3	π*C1-N4	305.54	LP(1) O7	1.97422
	LP(1) C3	σ*C16-C90	10.22	LP(2) O7	1.86496
	LP(1) O7	RY*C2	16.17	LP(1) N19	1.67360
	LP(2) O7	σ*C2-C16	24.23	LP(2) O92	1.83827
	LP(1) N19	π*C17-N18	31.96	C58-C60	0.39173
	LP(1) N19	π*C20-C22	35.39	C31-C32	0.38139
	LP(2) O92	π*C83-C87	31.07	-	-
	π*C17-N18	π*C31-C32	176.14	-	-
	π*C58-C60	π*C59-C61	245.71	-	-
3	πC1-N4	π*C1-N4	10.12	C1-N4	1.93843
	πC31-C32	π*C17-N18	19.06	C31-C32	1.63938
	πC82-C85	π*C83-C87	24.18	C82-C85	1.66571
	LP(1) C3	π*C1-N4	236.58	LP(1) C3	1.17909
	LP(1) N55	π*C53-N56	26.95	LP(1) N55	1.72380
	LP(1) N55	π*C58-C60	14.33	LP(1) F92	1.92286
	LP(1) F92	π*C45-C49	18.98	C31-C32	0.38498
	π*C17-N18	π*C31-C32	134.78	C45-C49	0.37223
	π*C45-C49	π*C44-C47	295.68	-	-
4	πC1-N4	LP(1) C3	17.68	C1-N4	1.94219
	LP(1) C3	π*C1-N4	210.17	LP(1) C3	1.21178
	LP(1) N55	π*C53-N56	29.59	LP(1) N55	1.72260
	LP(1) N55	π*C58-C60	10.77	C31-C32	0.38895
	π*C17-N18	π*C31-C32	130.35	C45-C49	0.36457
	π*C45-C49	π*C42-C43	291.80	-	-
5	LP(1) C3	π*C1-N4	235.32	LP(1) C3	1.17975
	LP(1) Cl92	π*C45-C49	12.44	LP(1) Cl91	1.92682
	π*C17-N18	π*C31-C32	127.50	C31-C32	0.38478
	π*C83-C87	π*C80-C81	248.24	C83-C87	0.39465

[a] E^2 means energy of hyperconjugative interactions (stabilization energy); $LP_{(n)}$ is a valence lone pair orbital (n) on atom.

In dioxane, the experimental spectrum is composed of two bands, at 343 and 298 nm. Increasing solvent polarity from dioxane to ethanol results in a blue shift of the two bands, where the first band is shifted to 339 nm, and the second band is shifted to 295 nm, respectively. Furthermore, increasing solvent polarity causes a marked increase in the intensity of both bands. The two observed bands are assigned as π → π* transitions, based on the values of molar absorptive (ε = 0.000-60.000). The interpretation of the experimentally observed UV spectra of compound **2** in dioxane and ethanol requires the theoretical calculations of the vertical transitions using CAM/B3LYP/6-311G(d,p) level. In dioxane, the band appearing in the experimental spectrum at 343 nm is reproduced theoretically using dioxane as a solvent at 336.3 nm (State I), as shown in Table S2, which involves orbital's φ_{196} and φ_{199}, showing a good agreement between the observed wavelength with the calculated wavelength. Theoretical gas phase calculations of compound **2** give a vertical excitation at 336.1 nm (State I), which is about 7.1 nm lower than the experimental wavelength, where the transition in the gas phase also involves the same orbitals. Increasing solvent polarity results in a blue shift of λ_{max} of this band to 339 nm. The theoretical calculations of the vertical excitation in ethanol reproduce the wavelength of this band at 335.4 nm (State I), indicating that the same orbital's are involved in this transition. It is also clear that the calculated wave length is lower than the observed wavelength. The second band theoretically at 320.0 nm (State II) in dioxane, indicating that the orbital's φ_{198} and φ_{201} are involved in this transition. Theoretical gas phase calculations give a wavelength at 320.8

nm (State II). This same band in ethanol at 325.3 nm (State II), where the same orbital's are involved in this transition. The third band theoretically at 304.2 nm (State III) in dioxane, indicating that the orbital's φ_{197} and φ_{200} are involved in this transition. Theoretical gas phase calculations give a wavelength at 303.6 nm (State III), this same band at 303.5 nm in ethanol. The fourth state (π-π*)[1], which observed at 298 nm in dioxane, is reproduced theoretically at 292.1 nm (State IV), where the calculations in dioxane indicate that the orbital's φ_{198} and φ_{202} are involved in this transition. Gas phase calculations give λ_{max} at 291.8 nm (State IV). Theoretical calculations in ethanol show that, this band appears at 292.3 nm (State IV), which is lower than the experimental wavelength. Theoretical gas phase wavelength is found to be lower than the observed wavelength in ethanol. The five band theoretically at 276.3 nm (State V) in dioxane, indicating that the orbital's φ_{198} and φ_{202} are involved in this transition. Theoretical gas phase calculations give a wavelength at 273.2 nm (State V). This same band in ethanol at 274.1 nm (State V), where the same orbital's are involved in this transition. The seven orbital's φ_{196}, φ_{197}, φ_{198}, φ_{199}, φ_{200}, φ_{201}, and φ_{202}, respecttively, involved in the theoretical transitions of compound **2**, are shown in Figure S2. The first band which involves φ_{196} and φ_{199} has electron density delocalization, while orbital's φ_{197}, φ_{198}, φ_{200}, φ_{201}, and φ_{202} have a Charge Transfer CT character. The results of NBO analysis of compound **2** tabulated in Table 5 indicate that there is a strong hyper conjugative interactions LP(1) $C_3 \rightarrow \pi^*C_1$-N_4, π^*C_{58}-$C_{60} \rightarrow \pi^*C_{59}$-$C_{61}$, π^*C_{17}-$N_{18} \rightarrow \pi^*C_{31}$-$C_{32}$, LP(1) $N_{19} \rightarrow \pi^*C_{20}$-$C_{22}$,
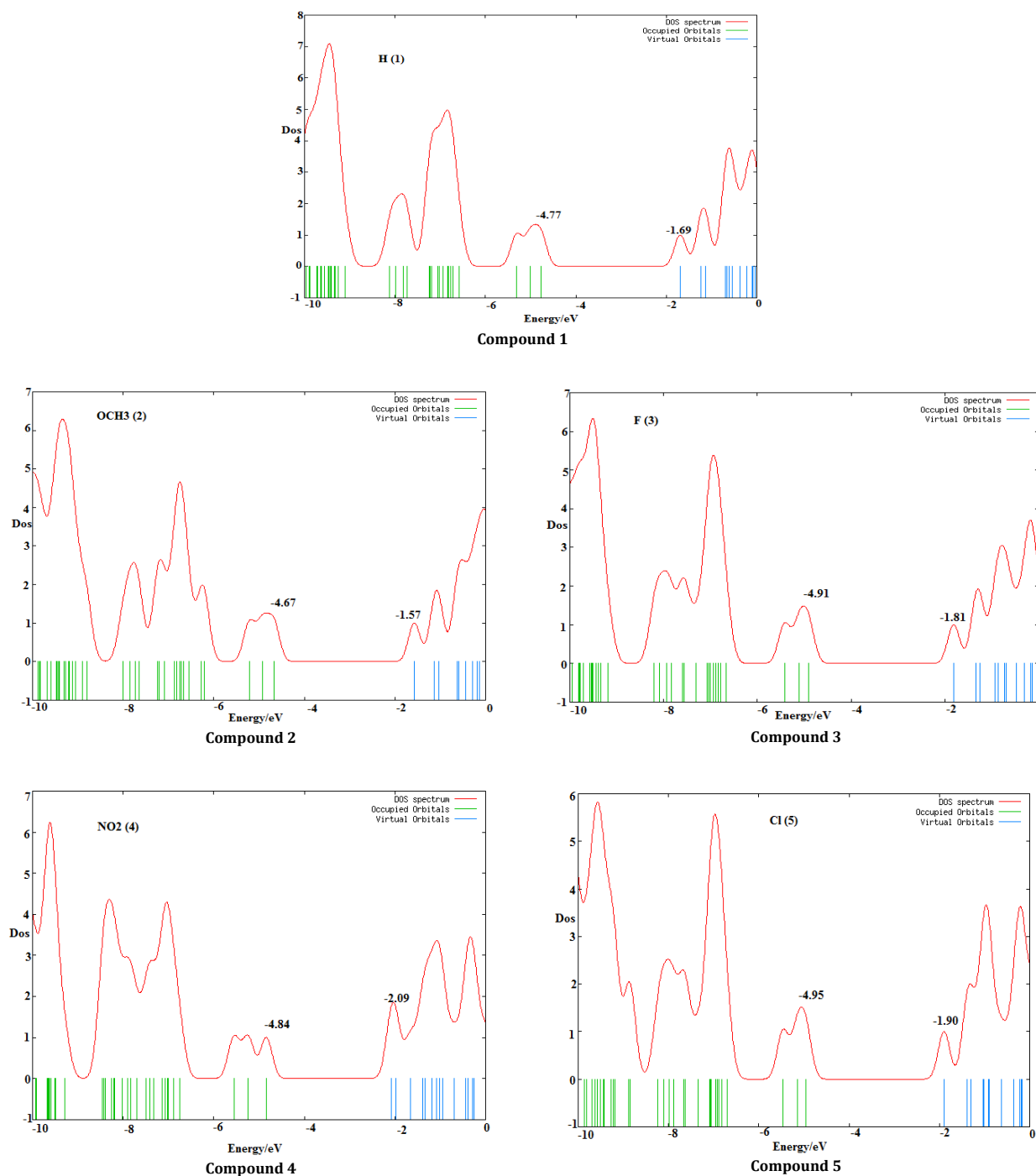
Figure 7. HOMOs, LUMOs and density of states (DOS) of the studied compounds **1**-**5** at B3LYP/6-311G(d,p) with Vertical Fermi levels.

LP(2) $O_{92} \rightarrow \pi^*C_{83}$-$C_{87}$, and LP(2) $O_7 \rightarrow \sigma^*C_2$-$C_{16}$, for compound **2** is 305.54, 245.71, 176.14, 35.39, 31.07 and 24.23 kcal/mol, respectively. NBO analysis of the *p*-OCH$_3$ derivative Table 5 indicates that it retained the extended conjugation of compound **1** as revealed by the interaction of C–N NBOs with those of pyrazole ring. Furthermore, the interaction of the oxygen lone orbital's with the C2–O7, C1–C57 and C3–C16 π^* orbital and σ^*C2–C16 is marked. The population of the NBO C58–C60, C31–C32, and LP(1) C$_3$ reflecting a charge transfer away from *bis*-spiropipridinon/pyrazole ring. This is also evident in the case of the population of the nitrogen lone orbital LP(1) N19.

3.9. Electronic absorption spectra of compound 3

To complete our investigation of substituent effect on the electronic structure and spectra of compound **1**, we introduce two F-groups in position two X in two Ph-X of compound **1** gives compound **3**. The experimental and theoretical elect-ronic absorption spectra of compound **3** in dioxane and ethanol are shown in Figure 11 and Table S3. The experimen-tal spectrum in dioxane is composed of two bands at 348 and 297 nm. The change of solvent polarity from dioxane to ethanol results in a blue shift of the two bands, where the first band is shifted to 344 nm, and the second band is shifted to 293 nm, respectively.
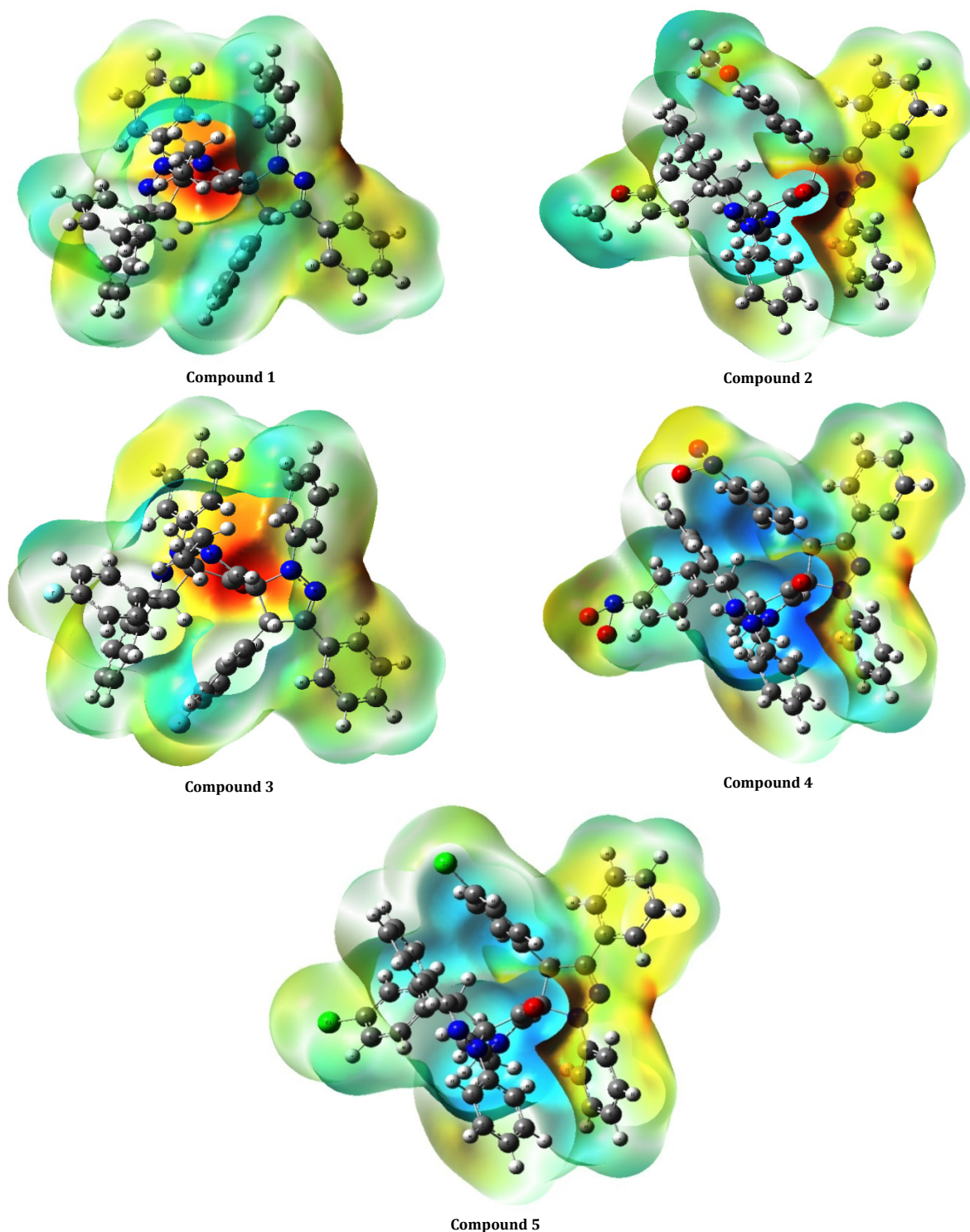
Figure 8. 3D MEP of the studied compounds **1-5** at B3LYP/6-311G(d,p). The color scheme for the MEP surface is as follows: red for electron rich, (partially negative charge); blue for electron deficient, (partially positive charge); light blue for (slightly electron deficient region); yellow for (slightly electron rich region); green for neutral (zero potential) respectively. Potential increases in the following order: red < orange < yellow < green < blue [49,50].

Furthermore, increasing solvent polarity causes a marked increase in the intensity of both bands. The values of molar absorptive (ε = 0.000-60.000) indicates that the two observed bands have $\pi \rightarrow \pi^*$ character. The theoretical vertical transitions using CAM/B3LYP/6-311G d,p) level is valuable for the analysis of the experimental UV spectra of compound **3** in dioxane and ethanol, which gives values for λ_{max} of 339.4 nm (State I) for the first band, 311.4 nm (State II) for the second band, 302.2 nm (State III) for the third band, and 289.9 nm (State IV) for the four band as shown in Table S3. Theoretical transitions in the gas phase give a vertical excitation at 339.7 nm (State I), which is about 8.3 nm lower than the experimental wavelength, where it involves the same orbitals as in dioxane. Theoretical vertical excitation calculations in ethanol give λ_{max} of this band at 337.4 nm (State I), which shows a fair agreement, implying that the orbitals involved in
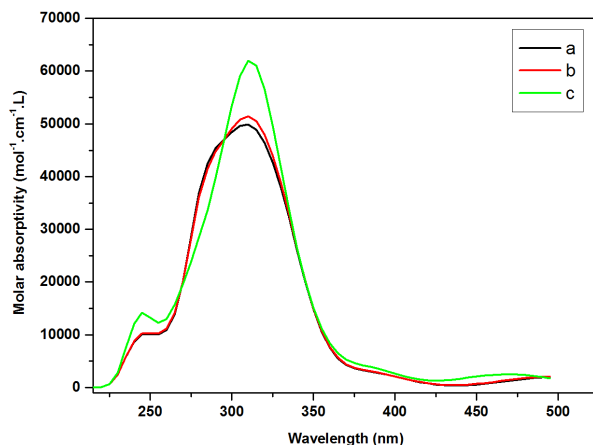
Figure 9. Electronic absorption spectra of compound **1**, (a) theoretical in gas phase, (b) theoretical in ethanol, (c) theoretical in dioxane.
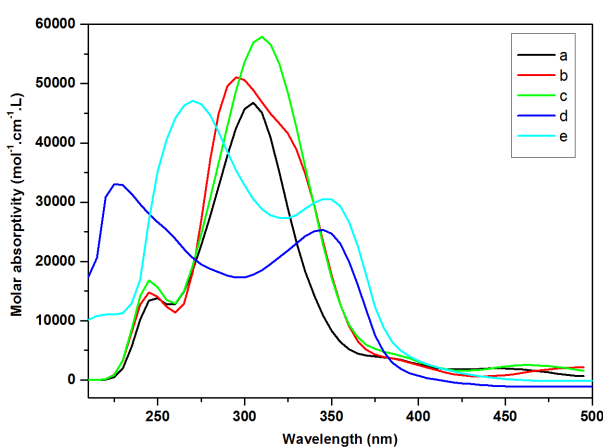

Figure 10. Electronic absorption spectra of compound **2**, (a) theoretical in gas phase, (b) theoretical in ethanol, (c) theoretical in dioxane, (d) experimental in ethanol, (e) experimental in dioxane.
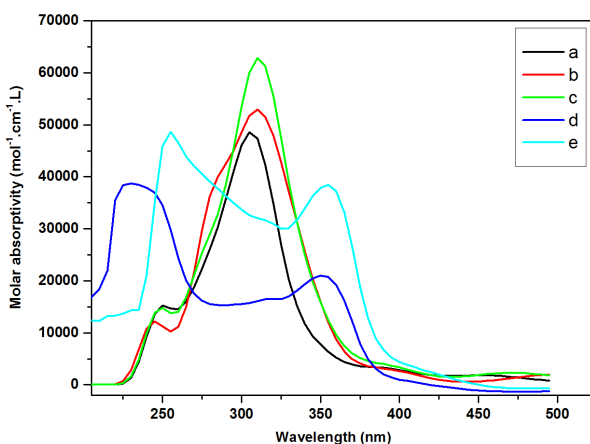

Figure 11. Electronic absorption spectra of compound **3**, (a) theoretical in gas phase, (b) theoretical in ethanol, (c) theoretical in dioxane, (d) experimental in ethanol, (e) experimental in dioxane.

this transition are φ_{188} and φ_{191}. The second band in dioxane, theoretically at 311.4 nm (State II), indicate that the orbital's φ_{190} and φ_{193} are involved in this transition. Gas phase calculations give λ_{max} at 313.7 nm (State II). Theoretical calculations in ethanol show that, this band appears at 314.6 nm (State II).

The third state $(\pi-\pi^*)^1$, in dioxane, theoretically at 302.2 nm (State III), indicate that the orbital's φ_{190} and φ_{192} are involved in this transition. Gas phase calculations give λ_{max} at

306.6 nm (State III). Theoretical calculations in ethanol show that, this band appears at 305.8 nm (State III). The four band (State IV), which observed at 297 nm in dioxane, is reproduced theoretically at 289.9 nm (State IV). Gas phase calculations give λ_{max} at 288.3 nm (State IV). Theoretical calculations in ethanol show that, this band appears at 289.3 nm (State IV). The eight orbital's φ_{188}-φ_{195} involved in the theoretical transitions of compound **3**, are shown in Figure S3 where these bands shows a CT character, electron density delocaliza-
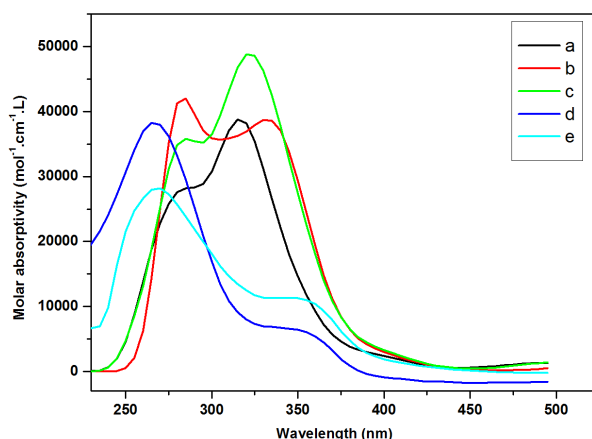
Figure 12. Electronic absorption spectra of compound **4**, (a) theoretical in gas phase, (b) theoretical in ethanol, (c) theoretical in dioxane, (d) experimental in ethanol, (e) experimental in dioxane.

tion, and localization. The results of NBO analysis of compound **3** tabulated in Table 5 indicate that there is a strong hyper conjugative interactions π^*C_{45}-$C_{49} \rightarrow \pi^*C_{44}$-$C_{47}$, LP(1) $C_3 \rightarrow \pi^*C_1$-N_4, π^*C_{17}-$N_{18} \rightarrow \pi^*C_{31}$-$C_{32}$, LP(1) $N_{55} \rightarrow \pi^*C_{53}$-$N_{56}$, π^*C_{82}-$C_{85} \rightarrow \pi^*C_{83}$-$C_{87}$, and LP(1) $F_{92} \rightarrow \sigma^*C_{45}$-$C_{49}$, for compound **3** is 295.68, 236.58, 134.78, 26.95, 24.18 and 18.98 kcal/mol, respectively. NBO analysis of the *p*-F derivative Table 5 indicates that it retained the extended conjugation of compound **1** as revealed by the interaction of C–N NBOs with those of pyrazole ring. Furthermore, the interaction of the F orbital's with C2–O7, C1–C57 and C3–C16 π^* orbital and σ^*C2–C16 is marked. The population of the NBO C45–C49, C31–C32, and LP(1) C_3 reflecting a charge transfer away from *bis*-spiropipridinon/pyrazole.

3.10. Electronic absorption spectra of compound 4

Compound **4** results by inserting two NO₂-atom in position two X in two Ph-X of compound **1**. The experimental and theoretical electronic absorption spectra of compound **4** in dioxane and ethanol are shown in Figure 12 and Table S4. The experimental spectrum in dioxane is composed of two bands at 355 and 295 nm. The change of solvent polarity from dioxane to ethanol results in a small red shift by 3 nm of the first band, and the second band. Additionally, increasing solvent polarity causes a marked decrease in the intensity of both bands. The values of molar absorptive (ε = 0.000-50.000) indicates that the two observed bands have π-π^* character. The theoretical vertical transitions using CAM/B3LYP/6-311G(d,p) level is valuable for the analysis of the experimental UV spectra ofcomopound **4** in dioxane and ethanol, which gives values for λ_{max} of 349.9 nm (State I) for the first band, 324.9 nm (State II) for the second band, 313.5 nm (State III) for the third band, 292.5 nm (State IV) for the fourth band and 274.3 nm (State V) for the five band as shown in Table S4. The theoretical transition of the first band in dioxane involves orbital's φ_{202} and φ_{205}, showing a good agreement between the observed and the calculated wavelengths. Theoretical transitions in the gas phase give a vertical excitation at 348.3 nm (State I), which is about 9.7 nm lower than the experimental wavelength, where it involves the same orbitals as in dioxane. Theoretical vertical excitation calculations in ethanol give λ_{max} of this band at 347.4 nm (State I), which shows a fair agreement, implying that the orbitals involved in this transition are φ_{202} and φ_{205}. The second band theoretically at 324.9 nm (State II) in dioxane, indicating that the orbital's φ_{204} and φ_{209} are involved in this transition. Theoretical gas phase calculations give a wavelength at 321.9 nm (State II). This

same band in ethanol at 323.9 nm (State II), where the same orbital's are involved in this transition. The third band theoretically at 313.5 nm (State III) in dioxane, indicating that the orbital's φ_{204} and φ_{208} are involved in this transition. Theoretical gas phase calculations give a wavelength at 311.7 nm (State III), this same band at 310.5 nm in ethanol. The fourth state (π-π^*)[1], which observed at 295 nm in dioxane, is reproduced theoretically at 292.5 nm (State IV), where the calculations in dioxane indicate that the orbital's φ_{204} and φ_{214} are involved in this transition. Gas phase calculations give λ_{max} at 290.0 nm (State IV).

Theoretical calculations in ethanol show that, this band appears at 291.1 nm (State IV), which is lower than the experimental wavelength. Theoretical gas phase wavelength is found to be lower than the observed wavelength in ethanol. The five band theoretically at 274.3 nm (State V) in dioxane, indicating that the orbital's φ_{203} and φ_{214} are involved in this transition. Theoretical gas phase calculations give a wavelength at 273.8 nm (State V). This same band in ethanol at 273.6 nm (state V), where the same orbital's are involved in this transition. The eight orbital's φ_{202}-φ_{205}, φ_{207}-$\varphi_{209,}$ and φ_{214} involved in the theoretical transitions of compound **4**, are shown in Figure S4 where these bands shows a CT character, electron density delocalization, and localization. The results of NBO analysis of compound **4** tabulated in Table 5 indicate that there is a strong hyper conjugative interactions π^*C_{45}-$C_{49} \rightarrow \pi^*C_{42}$-$C_{43}$, LP(1) $C_3 \rightarrow \pi^*C_1$-N_4, π^*C_{17}-$N_{18} \rightarrow \pi^*C_{31}$-$C_{32}$,and LP(1) $N_{55} \rightarrow \pi^*C_{53}$-$N_{56}$, for compound **4** is 291.80, 210.17, 130.35, and 29.59 kcal/mol, respectively. NBO analysis of the *p*-NO₂ derivative Table 5 indicates that it retained the extended conjugation of compound **1** as revealed by the interaction of C–NO₂ NBOs with those of both phenyl rings. Furthermore, the interaction of the NO₂ orbital's with the C2–C16 σ^* orbital is marked. The population of the NBO C45–C49, C31–C32, and LP(1) C_3 reflecting a charge transfer away from *bis*-spiropipridinon/pyrazole.

3.11. Electronic absorption spectra of compound 5

Introducing two Cl-atom in position two X in two Ph-X of compound **1**, results in the formation of compound **5**. The experimental and theoretical electronic absorption spectra of compound **5** in dioxane and ethanol are shown in Figure 13 and Table S5. The experimental spectrum of compound **5** in dioxane is composed of two bands appearing at 353 and 298 nm, respectively. Compound **5** in ethanol exhibits two bands at 349 and 295 nm. The change of solvent polarity results in a slight blue shift for all bands.

Table 6. Antimicrobial activity for the studied compounds **2-5**.

Compounds	Diameter of inhibition zone (mm) at conc. of µg/mL				
	Gram (+)		Gram (-)		Fungus
	S. aureus	*E. coli*	*K. pneumonia*	*P. vulgaris*	*C. albicans*
2	10	9	10	10	10
3	11	10	9	11	12
4	17	18	15	19	16
5	12	11	10	12	12
Doxymycin [a]	14	15	15	15	-
Fluconazole [b]	-	-	-	-	14

[a] Antibacterial standard.
[b] Antifungal standard.
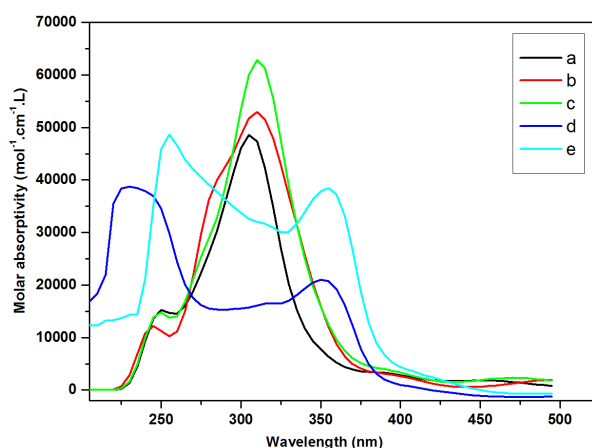
Figure 13. Electronic absorption spectra of compound **5**, (a) theoretical in gas phase, (b) theoretical in ethanol, (c) theoretical in dioxane, (d) experimental in ethanol, (e) experimental in dioxane.

The intensity of all bands is increase upon increasing solvent polarity. All bands are assigned to have π-π* character. The observed UV spectra of compound **5** in dioxane is interpreted by using CAM/B3LYP/6-311G(d,p) vertical excitation calculations, which gives excitations at 342.9 nm (State I), 311.1 nm (State II), 303.5 nm (State III), 292.6 nm (State IV), and 276.8 nm (state V) nm, respectively, which shows a good agreement with the observed spectra. The theoretical transition of the first band in dioxane involves orbital's φ_{196} and φ_{199}, showing a good agreement between the observed and the calculated wavelengths. Theoretical transitions in the gas phase give a vertical excitation at 343.5 nm (State I), which is about 9.5 nm lower than the experimental wavelength, where it involves the same orbitals as in dioxane. Theoretical vertical excitation calculations in ethanol give λ_{max} of this band at 340.6 nm (state I), which shows a fair agreement, implying that the orbitals involved in this transition are φ_{196} and φ_{199}. The second band theoretically at 311.1 nm (State II) in dioxane, indicating that the orbital's φ_{197} and φ_{200} are involved in this transition. Theoretical gas phase calculations give a wavelength at 313.5 nm (State II). This same band in ethanol at 315.3 nm (State II), where the orbital's φ_{198} and φ_{201} are involved in this transition. The third band theoretically at 303.5 nm (State III) in dioxane, indicating that the orbital's φ_{198} and φ_{200} are involved in this transition. Theoretical gas phase calculations give a wavelength at 306.3 nm (State III), this same band at 306.0 nm in ethanol. The fourth state (π-π*)[1], which observed at 298 nm in dioxane, is reproduced theoretically at 292.6 nm (State IV), where the calculations in dioxane indicate that the orbital's φ_{198} and φ_{202} are involved in this transition. Gas phase calculations give λ_{max} at 290.3 nm (state IV). Theoretical calculations in ethanol show that, this band appears at 293.3 nm (state IV), which is lower than the experimental wavelength. Theoretical gas phase wavelength is found to be lower than the observed wavelength in ethanol. The five band theoretically at 276.8 nm (State V) in dioxane, indicating that the orbital's φ_{198} and φ_{202} are involved in this

transition. Theoretical gas phase calculations give a wavelength at 273.8 nm (State V). This same band in ethanol at 275.6 nm (state V), where the same orbital's are involved in this transition. The seven orbital's φ_{196}-φ_{202}, involved in the theoretical transitions of compound **5**, are shown in Figure S5 where these bands shows a CT character, electron density delocalization, and localization. The results of NBO analysis of compound **5** tabulated in Table 5 indicate that there is a strong hyper conjugative interactions π*C$_{83}$-C$_{87}$ → π*C$_{80}$-C$_{81}$, LP(1) C$_3$ → π*C$_1$-N$_4$, π*C$_{17}$-N$_{18}$ → π*C$_{31}$-C$_{32,}$ and LP(1) Cl$_{92}$ → π*C$_{45}$-C$_{49}$, for compound **5** is 248.24, 235.32, 127.50 and 12.44 kcal/mol, respectively. NBO analysis of the *p*-Cl derivative Table 5 indicates that it retained the extended conjugation of compound **1** as revealed by the interaction of C–Cl NBOs with those of both phenyl rings. Furthermore, the interaction of the Cl orbital's with the C2–C16 σ* orbital is marked. The population of the NBO C83–C87, C31–C32, and LP(1) C$_3$ reflecting a charge transfer away from *bis*-spiro-pipiridinon/ pyrazole.

3.12. Antimicrobial activity

Biological activities of synthesized *bis*-spiropipridinon/ pyrazole derivatives compounds were studied for antibacterial and antifungal properties against different types of bacteria; Gram positive *S. aureus*, and *E. coli* and Gram negative *K. pneumonia* and *P. vulgaris*, and *C. albicans* for fungus. Results were recorded by measuring the growth inhibition (zone of inhibition) surrounding the disc of material. Results of MIC are summarized in Table 6. Some antibiotics were evaluated for their antibacterial activities and their results were found ineffective to all bacteria and fungus. Compound **2** show weak activity except for both compounds **4**, **5** and **3** is quite effective against *E. coli*, *P. vulgaris*, and *C. albicans*. Antimicrobial activity results revealed that compound **4** has a good potency against all Gram-positive bacteria especially *E. coli* and all Gram-negative bacteria especially *P. vulgaris* in comparison

with doxymycin standard. Those compounds **2-5** give more explanation of the high antimicrobial activity against all tested bacteria and fungi in which the small size of compound **4** increases its absorption ability on the surface of the cell wall of microorganisms and the respiration process of the cell. Hence, compound **4** is essential for the growth-inhibitor effect.

3.13. Structure activity relationship (SAR)

The biological activity of the *bis*-spiropipridinon/pyrazole derivatives can be correlated with the ground state energetic and global properties. From the computed data in Tables 3 and 6, one can reveal the following:

1. The reactivity of *bis*-spiropipridinon/pyrazole derivatives follow the order $NO_2 < Cl < F < OCH_3$, Against Gram(+), Gram(-) and fungi. The reactivity can be explained in terms of the energy gap, E_{HOMO} which measures the donating power and dipole moment which measure the charge separation.
2. Theoretically, the order of the energy gap $NO_2 < Cl < F < OCH_3$, the order of E_{HOMO} $NO_2 < Cl < F < OCH_3$, and the order of the dipole moment $NO_2 < Cl < F < OCH_3$ which are of the same order of the reactivity of *bis*-spiropipridinon /pyrazole derivatives towards Gram(+), Gram(-) and fungi. In conclusions, the substituent in the studied compounds **2**-**5** increases with its biological activity.

4. Conclusion

The molecular geometry of *bis*-spiropipridinon/pyrazole derivatives in the ground state has been calculated by using DFT-B3LYP/6-311G(d,p) level of theory. The optimized structure of the studied compounds **1-5** are non-planner with the two phenyl at C53 and C92 are out of the molecular plane of *bis*-spiropipridinon/pyrazole by a dihedral angles of 91.67 and 19.79°, respectively. The small difference between E_g of the studied compounds **1**-**5** may be attributed to the presence of the two Ph-X and Ph-X out of the molecular plane of *bis*-spiropipridinon/pyrazole moiety. The density of states, the chemical reactivity, hardness, softness, chemical potential and electro negativity analyzed by the HOMO-LUMO energy gap. Mullikan and natural charge distribution of the molecule were studied which indicated the electronic charge distribution in the molecule. The first order hyperpolarizability and the calculated dipole moment results indicate that the molecule has a reasonable good non-linear optical behavior. The total electron density surface with MEP confirmed the different negative and positive potential sites of the molecule. Electronic absorption spectra are investigated experimentally in dioxane and ethanol; and theoretically in gas phase, dioxane and ethanol using CAM-B3LYP/6-311G(d,p). Compounds **2-5** exhibit 2 bands, in both solvents, while compound **1** exhibit 6 bands theoretically only due to expensive to prepare compound. The band maxima (λ_{max}) and intensities of the spectra are found to have solvent dependence. The bands of compounds **2**, **3**, and **5** show blue shift, while compound **4** show red shift. Theoretical calculations of the vertical excitations at the CAM-B3LYP/6-311G(d,p) reproduce the experimental spectra, indicating a good agreement between theory and experiment. The NBO analysis of the compounds **1-5** indicated the intermolecular charge transfer between the bonding and antibonding orbital's. Novel *bis*-spiropipridinon/ pyrazolederivatives were tested as antimicrobial agents. Experimental results indicate that compound **4** is a useful anti-microbial agent for different bacteria and fungus. Compound **4** was found to be more reactive and more polar than other compounds. Theoretically, reactivity of the studied compounds follows the order: $NO_2 < Cl < F < OCH_3$, which is the same order of reactivity towards Gram(+), Gram(-), and fungus.

Supporting information Ⓢ

The online version of this article contains supplementary material, which is available to authorized users.

Disclosure statement

Conflict of interests: The authors declare that they have no conflict of interest.
Author contributions: All authors contributed equally to this work.
Ethical approval: All ethical guidelines have been adhered.
Sample availability: Samples of the compounds are available from the author.

ORCID ⒾⒹ

Shimaa Abdel Halim
ⒾⒹ http://orcid.org/0000-0003-3926-193X

References

[1]. Kobayashi, J.; Tsuda, M.; Agemi, K.; Shigemori, H.; Ishibashi, M.; Sasaki, T.; Mikami, Y.; Purealidins, B . *Tetrahedron* **1991**, *47*, 6617-6622.
[2]. James, D. M.; Kunze, H. B.; Faulkner, D. J. *J. Nat. Prod.* **1991**, *54*, 1137-1140.
[3]. Hilton, S. T.; Ho, T. C.; Pljevalijcic, G.; Jones, K. A. *Org. Lett.* **2000**, *17*, 2639-2641.
[4]. Pavlovska, T. L.; Redkin, R. G.; Lipson, V. V.; Atamanuk, D. V. *Mol. Divers.* **2016**, *20*, 299-344.
[5]. Urman, H. K.; Bulay, O.; Clayson, D. B.; Shubik, P. *Cancer Lett.* **1975**, *1*, 69-74.
[6]. Duksin, D.; Katchalski, E.; Sachs, L. *Proc. Natl. Acad. Sci.* **1970**, *67(1)*, 185-192.
[7]. Field, A. K.; Tytell, A. A.; Lampson, G. P.; Hilleman, M. R. *Proc. Natl. Acad. Sci. USA* **1967**, *58(3)*, 1004-1010.
[8]. Reddy, C.; Rao, L.; Nagaraj, A. *Acta Chim. Slov.* **2010**, *57*, 798-807.
[9]. Kheder, N. A.; Mabkhot, Y. N. *Int. J. Mol. Sci.* **2012**, *13(3)*, 3661-3670.
[10]. Abou-Seri, S. M. *Eur. J. Med. Chem.* **2010**, *45(9)*, 4113-4121.
[11]. Abdelmoniem, A.; Elwahy, A. H. M.; Abdelhamid, I. A. *Arkivoc* **2016**, *3*, 304-312.
[12]. Cravotto, G.; Giovenzana, G. B.; Pilati, T.; Siste, M.; Palmisano, G. *J. Org. Chem.* **2001**, *66*, 8447-8453.
[13]. Daly, J. W.; Spande, T. W.; Whittaker, N.; Highet, R. J.; Feigl, D.; Noshimori, N.; Tokuyama, T.; Meyers, C. W. *J. Nat. Prod.* **1986**, *49*, 265-280.
[14]. Waldmann, H. *Syn. Let.* **1995**, 133-141.
[15]. Weber, L. *Drug Discov. Today* **2002**, *7*, 143-147.
[16]. Domling, A. *Curr. Opin. Chem. Biol.* **2002**, *6*, 306-313.
[17]. Hassaneen, H. M. E.; Eid, E. M.; Eid, H. A.; Farghaly, T. A.; Mabkhot, Y. M. *Molecules* **2017**, *22*, 357-372.
[18]. Abunada, N. M.; Hassaneen, H. M.; Kandile, N. G.; Miqdad, O. A. *Molecules* **2008**, *13*, 1501-1517.
[19]. Ezawa, M.; Garvey, D. S.; Janero, D. R.; Khanapure, S. P.; Letts, L. G.; Martino, A.; Ranatunge, R. R.; Schwalb, D. J.; Young, D. V. *Lett. Drug Design Discov.* **2005**, *2*, 40-43.
[20]. Suleyman, H.; Buyukokuroglu, M. E. *Biol. Pharm. Bull.* **2001**, *24(10)*, 1133-1136.
[21]. Abadi, A. H.; Eissa, A. A. H.; Hassan, G. S. *Chem. Pharm. Bull.* **2003**, *51(7)*, 838-844.
[22]. Mohan, S.; Ananthan, S.; Murugan, K. R. *Intern. J. Pharma Sci. Res.* **2010**, *1(9)*, 391-398.
[23]. Jamwal, A.; Javed, A.; Bhardwaj, V. *J. Pharm. Bio. Sci.* **2013**, *3*, 114-123.
[24]. Kvashnin, Y. A.; Kazin, N. A.; Verbitskiy, E. V.; Svalova, T. S.; Ivanova, A. V.; Kozitsina, A. N.; Slepukhin, P. A.; Rusinov, G. L.; Chupakhin, O. N.; Charushina, V. N. *Arkivoc* **2016**, *5*, 279-300.
[25]. Asif M. *Chem. Intern.* **2015**, *1(3)*, 134-163.
[26]. Samshuddin, S.; Narayana, B.; Sarojini, B. K.; Srinivasan, R.; Chandrashekar, K. R. *Der Pharma Chem. ,* **2012**, *4(2)*, 587-592.
[27]. Pinto, D. C. G. A.; Santos, C. M. M.; Silva, A. M. S. Advance NMR techniques for structural characterization of heterocyclic structures,

Recent Research Developments in Heterocyclic Chemistry, Capitulo 8, pp. 397-475, Research Signpost, Kerala, India, 2007.

[28]. Dawood, K. M. *J. Heterocyclic Chem.* **2005**, *42*, 221-225.
[29]. Becke, A. D. *J. Chem. Phys.* **1993**, *98*, 5648-5652.
[30]. Lee C.; Yang, W.; Parr, R. G. *Phys. Rev. B Condens. Matter.* **1988**, *37*, 785-789.
[31]. Frisch, M. J.; Trucks, G. W.; Schlegel, H. B.; Scuseria, G. E.; Robb, M. A.; Cheeseman, J. R.; Montgomery, Jr. , J. A.; Vreven, T.; Kudin, K. N.; Burant, J. C.; Millam, J. M.; Iyengar, S. S.; Tomasi, J.; Barone, V.; Mennucci, B.; Cossi, M.; Scalmani, G.; Rega, N.; Petersson, G. A.; Nakatsuji, H.; Hada, M.; Ehara, M.; Toyota, K.; Fukuda, R.; Hasegawa, J.; Ishida, M.; Nakajima, T.; Honda, Y.; Kitao, O.; Nakai, H.; Klene, M.; Li, X.; Knox, J. E.; Hratchian, H. P.; Cross, J. B.; Bakken, V.; Adamo, C.; Jaramillo, J.; Gomperts, R.; Stratmann, R. E.; Yazyev, O.; Austin, A. J.; Cammi, R.; Pomelli, C.; Ochterski, J. W.; Ayala, P. Y.; Morokuma, K.; Voth, G. A.; Salvador, P.; Dannenberg, J. J.; Zakrzewski, V. G.; Dapprich, S.; Daniels, A. D.; Strain, M. C.; Farkas, O.; Malick, D. K.; Rabuck, A. D.; Raghavachari, K.; Foresman, J. B.; Ortiz, J. V.; Cui, Q.; Baboul, A. G.; Clifford, S.; Cioslowski, J.; Stefanov, B. B.; Liu, G.; Liashenko, A.; Piskorz, P.; Komaromi, I.; Martin, R. L.; Fox, D. J.; Keith, T.; Al-Laham, M. A.; Peng, C. Y.; Nanayakkara, A.; Challacombe, M.; Gill, P. M. W.; Johnson, B.; Chen, W.; Wong, M. W.; Gonzalez, C.; Pople, J. A. Gaussian 03, Revision C. 02, Gaussian, Inc. , Wallingford CT, 2004.
[32]. Frisch, M. J.; Trucks, G. W.; Schlegel, H. B.; Scuseria, G. E.; Robb, M. A.; Cheeseman, J. R.; Scalmani, G.; Barone, V.; Mennucci, B.; Petersson, G. A.; Nakatsuji, H.; Caricato, M.; Li, X.; Hratchian, H. P.; Izmaylov, A. F.; Bloino, J.; Zheng, G.; Sonnenberg, J. L.; Hada, M.; Ehara, M.; Toyota, K.; Fukuda, R.; Hasegawa, J.; Ishida, M.; Nakajima, T.; Honda, Y.; Kitao, O.; Nakai, H.; Vreven, T.; Montgomery, J. A. Jr.; Peralta, J. E.; Ogliaro, F.; Bearpark, M.; Heyd, J. J.; Brothers, E.; Kudin, K. N.; Staroverov, V. N.; Kobayashi, R.; Normand, J.; Raghavachari, K.; Rendell, A.; Burant, J. C.; Iyengar, S. S.; Tomasi, J.; Cossi, M.; Rega, N.; Millam, J. M.; Klene, M.; Knox, J. E.; Cross, J. B.; Bakken, V.; Adamo, C.; Jaramillo, J.; Gomperts, R.; Stratmann, R. E.; Yazyev, O.; Austin, A. J.; Cammi, R.; Pomelli, C.; Ochterski, J. W.; Martin, R. L.; Morokuma, K.; Zakrzewski, V. G.; Voth, G. A.; Salvador, P.; Dannenberg, J. J.; Dapprich, S.; Daniels, A. D.; Farkas, Ö.; Foresman, J. B.; Ortiz, J. V.; Cioslowski, J.; Fox, D. J. Gaussian, Inc., Wallingford CT, 2009.

[33]. Dennington, R.; Keith, T. A.; Millam, J. M. GaussView, Version 5, Semichem Inc., Shawnee Mission KS, 2009.
[34]. Chemcraft - Graphical software for visualization of quantum chemistry computations. https://www.chemcraftprog.com
[35]. O'Boyle, N. M.; Tenderholt, A. L.; Langner, K. M. *J. Comput. Chem.* **2008**, *29*, 839-845.
[36]. Matecki J. G. *Trans. Met. Chem.* **2010**, *59*, 2764-2771.
[37]. Yanai, T.; Tew, D.; Handy, N. *Chem. Phys. Lett.* **2004**, *393*, 51-57.
[38]. Chocholousova, J.; Spirko, V.; Hobza, P. *Phys. Chem.* **2004**, *6*, 37-41.
[39]. Szafran, M.; Komasa, A.; Bartoszak-Adamska, E. *J. Mol. Struct.* **2007**, *827*, 101-107.
[40]. Avci, D. *Spectrochim. Acta A* **2011**, *82*, 37-43.
[41]. Avci, D.; Basoglu, A.; Atalay, Y. *Struct. Chem.* **2010**, *21*, 213-219.
[42]. Avci, D.; Comert, H.; Atalay, Y. *J. Mol. Mod.* **2008**, *14*, 161-171.
[43]. Pearson, R. G. *Proc. Nat. Acad. Sci.* **1986**, *83*, 8440-8441.
[44]. Chandra, A. K.; Uchimara, T. *J. Phys. Chem. A* **2001**, *105*, 3578 -3582.
[45]. El-Hiti, G. A.; Smith, K.; Hegazy, A. S.; Masmali, A. M.; Kariuki, B. M. *Acta. Cryst. E* **2014**, *70*, o932-o932.
[46]. El-Hiti, G. A.; Smith, K.; Hegazy, A. S.; Alanazi, S. A.; Kariuki, B. M. *Acta. Cryst. E* **2015**, *71*, o562-o563.
[47]. El-Hiti, G. A.; Smith, K.; Hegazy, A. S.; Ajarim, M. D.; Kariuki, B. M. *Acta. Cryst. E* **2015**, *71*, o877-o877.
[48]. Snehalatha, M.; Ravikumar, C.; Hubert, J. I.; Sekar, N.; Jayakumar, V. S. *Spectrochim. Acta A* **2009**, *72*, 654-662.
[49]. Bradshow, D. S.; Andrews, D. L. *J. Nonlinear Opt. Phys. Matter.* **2009**, *18*, 285-299.
[50]. Cheng, L. T.; Tam, W.; Stevenson, S. H.; Meredith, G. R.; Rikken, G.; Marder, S. R. *J. Phys. Chem.* **1991**, *95*, 10631-10643.
[51]. Kaatz, P.; Donley, E. A.; Shelton, D. P. *J. Chem. Phys.* **1998**, *108*, 849-856.
[52]. Gnanasambandan, T.; Gunasekaran, S.; Seshadri, S. *Spectrochim. Acta A* **2014**, *117*, 557-567.
[53]. Scrocco, E.; Tomasi, J. *J. Adv. Quant. Chem.* **1978**, *11*, 115-193.
[54]. Politzer, P.; Murray, J. S. *Theor. Chem. Acc.* **2002**, *108*, 134-142.
[55]. Sajan, D.; Josepha, L.; Vijayan, N.; Karabacak, M. *Spectrochim. Acta A* **2011**, *81*, 85-98.